



Wind-powered Ultraluminous X-ray Sources

Grzegorz Wiktorowicz^{1,2,3} , Jean-Pierre Lasota^{3,4} , Krzysztof Belczynski³, Youjun Lu^{1,2} , Jifeng Liu^{1,2,5}, and Krystian Iłkiewicz^{3,6,7}

¹National Astronomical Observatories, Chinese Academy of Sciences, Beijing 100101, People's Republic of China; gwiktoro@astrou.edu.pl

²School of Astronomy & Space Science, University of the Chinese Academy of Sciences, Beijing 100012, People's Republic of China

³Nicolaus Copernicus Astronomical Center, Polish Academy of Sciences, Bartycka 18, 00-716 Warsaw, Poland

⁴Institut d'Astrophysique de Paris, CNRS et Sorbonne Université, UMR 7095, 98bis Bd Arago, F-75014 Paris, France

⁵WHU-NAOC Joint Center for Astronomy, Wuhan University, Wuhan, People's Republic of China

⁶Centre for Extragalactic Astronomy, Department of Physics, University of Durham, South Road, Durham, DH1 3LE, UK

⁷Department of Physics and Astronomy, Box 41051, Science Building, Texas Tech University, Lubbock, TX 79409-1051, USA

Received 2021 March 2; revised 2021 June 18; accepted 2021 June 18; published 2021 September 8

Abstract

Although ultraluminous X-ray sources (ULX) are important for astrophysics because of their extreme apparent super-Eddington luminosities, their nature is still poorly known. Theoretical and observational studies suggest that ULXs could be a diversified group of objects that are composed of low-mass X-ray binaries, high-mass X-ray binaries and marginally also systems containing intermediate-mass black holes. Observational data on the ULX donors could significantly boost our understanding of these systems, but only a few have been detected. There are several candidates, mostly red supergiants (RSGs), but surveys are typically biased toward luminous near-infrared objects. In ULXs harbouring RSGs matter accreted onto the compact body would have to be provided by the stellar wind of the companion because a Roche-lobe overflow could be unstable for relevant mass-ratios. We present a comprehensive study of the evolution and population of wind-fed ULXs, and we provide a theoretical support for the link between RSGs and ULXs. Assuming a minimal model of stellar-wind emission, our estimated upper limit on contribution of wind-fed ULX to the overall ULX population is $\sim 75\%–96\%$ for young (<100 Myr) star-forming environments, $\sim 49\%–87\%$ for prolonged constant star formation (e.g., disk of Milky Way), and $\lesssim 1\%$ for environments in which star formation ceased long time (>2 Gyr) ago. We show also that some wind-fed ULXs (up to 6%) may evolve into merging double compact objects (DCOs). We demonstrate that the exclusion of wind-fed ULXs from population studies of ULXs might have led to systematic errors in their conclusions.

Unified Astronomy Thesaurus concepts: Black holes (162); Gravitational waves (678); Binary stars (154); X-ray binary stars (1811); Astrostatistics (1882); Astronomy databases (83)

1. Introduction

Ultraluminous X-ray sources (ULXs) are defined as point-like off-nuclear X-ray sources with luminosities exceeding 10^{39} erg s⁻¹ (for a recent review see Kaaret et al. 2017). Therefore, they are the brightest X-ray sources that are neither supernovae (SNe) nor active galactic nuclei. After their identification at the end of the previous century, it was thought for a long time that ULXs contain intermediate-mass ($M \sim 10^2–10^4 M_\odot$) black holes (IMBHs Colbert & Mushotzky 1999) that are accreting at rates close to or below their Eddington values. The dissenting view of King et al. (2001)—who pointed out that there are no viable evolutionary scenarios leading to the formation of such systems and instead suggested that most ULXs are stellar-mass binaries that are accreting at super-Eddington rates—was largely ignored until Bachetti et al. (2014) discovered that the source M82 ULX-2 contains an X-ray pulsar. This observation and the subsequent observations of five other pulsating ULXs (PULXs) by Israel et al. (2017), Fürst et al. (2017), Carpano et al. (2018), Sathyaprakash et al. (2019), Rodríguez Castillo et al. (2020) led to a change of paradigm and it is now universally believed that most (if not all) ULXs contain stellar-mass accretors. PULXs have been also observed during giant outbursts of Be-X-ray binary stars (one in the Galaxy, see King & Lasota 2020, and references therein), but their luminosities are always less than 3×10^{39} erg s⁻¹ (e.g., Tsygankov et al. 2017; Chandra et al. 2020).

The choice of the threshold ULX luminosity at 10^{39} erg s⁻¹ is rather unfortunate because it fails to separate the “standard” X-ray binaries (XRBs) from the “generic” ULX. Indeed, at least five transient galactic XRBs reach luminosities superior to 10^{39} erg s⁻¹ (Tetarenko et al. 2016). Middleton et al. (2015) suggest that one should take 3×10^{39} erg s⁻¹ as the minimum luminosity defining ULXs whose nature is “contentious” (i.e., that could contain either stellar-mass accretors or IMBHs). The idea was to make sure that if the accretor is a black hole (BH), then such a floor value would make sure that the apparent luminosity is super-Eddington. However, this suggestion does not take into account that it is now known that stellar evolution can produce BHs with masses $\gtrsim 30 M_\odot$ (Belczynski et al. 2010b; Abbott et al. 2016), and up to $50 M_\odot$ under favorable conditions (e.g., Belczynski 2020). Therefore, only sources with luminosities larger than $\sim 6 \times 10^{39}$ erg s⁻¹, for example, can be expected to be (apparently) super-Eddington if they contain a stellar-mass BH.⁸

Since the isotropic luminosity of an accreting body can be, at best, a few times its Eddington value (see, e.g., Shakura & Sunyaev 1973; Poutanen et al. 2007), observed luminosities $L \gg L_{\text{Edd}}$, where L_{Edd} is the Eddington luminosity, are only apparently super-Eddington and must be due to radiation beamed toward the observer (King et al. 2001; Abramowicz 2005). For example, in the model developed by King

⁸ The limit may even be higher for He-rich accretion and most massive BHs (e.g., Belczynski 2020).

(2009) radiation is collimated for $L \gtrsim 3 L_{\text{Edd}}$. One should realise that the beaming of apparently super-Eddington luminosities is unavoidable for neutron star (NS) accretors. In the case of NS ULXs, it has been speculated that magnetar-strength magnetic field ($B > 10^{13}$ G), by increasing the value of the threshold luminosity, would make the emission effectively sub-critical (cf Tong 2015; Dall’Osso et al. 2015; Eksi et al. 2015; Mushtukov et al. 2015). However, this hypothesis is contradicted by observations in several ULXs of cyclotron resonance scattering feature (CRSF), which corresponds to magnetic fields $B \sim 10^{11} - 10^{12}$ G (Brightman et al. 2018; Middleton et al. 2019; Walton et al. 2018), as well as by the absence of magnetars in binary systems, which is consistently explained by their formation scenarios invoking the destruction of the parent binary system (see King & Lasota 2019, and references therein). The importance of beaming in the context of the ULX origin and observed populations was recently analyzed by Wiktorowicz et al. (2019a).

Since the universal presence of extremely strong magnetic fields in NS ULXs is very unlikely and is impossible in BH ULXs, the observed luminosities $\gtrsim 3 \times 10^{39}$ erg s⁻¹ for NU LXs (we allow for the existence of NSs with masses $\approx 2.5 M_{\odot}$, Abbott et al. 2020), and larger than $\sim 6 \times 10^{39}$ erg s⁻¹ in general, cannot be intrinsic and must be beamed, as predicted by King et al. (2001). This requires high accretion rates⁹ typically $\dot{m} \equiv \dot{M}/\dot{M}_{\text{Edd}} \gtrsim 9$, where $\dot{M}_{\text{Edd}} = 2.0 \times 10^{-8} M_{\star} (0.1/\eta) M_{\odot} \text{ yr}^{-1}$, with η being the accretion efficiency and M_{\star} the accretor mass in solar units. Therefore, the accretion rate in bright ULXs ($L_{\text{X}} > 6 \times 10^{39}$ erg s⁻¹) should be larger than $\sim 1.8 \times 10^{-7} M_{\star} (0.1/\eta) M_{\odot} \text{ yr}^{-1}$. This is roughly the minimum rate at which accretion discs in (quasi)steady ULXs must be fed by the companion star. Some ULXs are transient (see, e.g., Earnshaw et al. 2020; Brightman et al. 2020). If this luminosity variability is due to the disk thermal-viscous instability, then the MT rate should be lower than the value mentioned above (Hameury & Lasota 2020).

The detection of a donor and its orbital motion can shed more light on the MT rates in a ULX and the nature of these objects. However, all ULXs, except potential Galactic ones such as SS433 and the Be-X source Swift J0243.66124, are extragalactic objects and their donors, if not very luminous, remain undetectable for contemporary surveys. Companion stars have only been dynamically confirmed in the case of two systems: 10–20 M_{\odot} B9Ia star in NGC7793 P13 (Motch et al. 2014) and $>3.4 M_{\odot}$ WR star in NGC 101 ULX-1 (Liu et al. 2013). Binary population studies suggest that the majority of ULXs are powered by low-mass and low-luminous donors, which is consistent with the lack of detection of any companions in the majority of ULXs. For example, Wiktorowicz et al. (2017) showed that the majority of ULXs will harbour $M < 3 M_{\odot}$ MS donors. Such stars are only observable in the vicinity of the Sun (even HST is constrained to the Milky Way in their case). Hyper-luminous X-ray sources, which are typically defined as ULXs with apparent luminosities above 10^{41} erg s⁻¹, are still viable candidates to harbour massive donors ($\gtrsim 10 M_{\odot}$; e.g., Wiktorowicz et al. 2015).

Several ULXs possess donor candidates spatially that are coincident with X-ray sources. Most of them were detected through observations in the near-infrared (NIR) spectral band.

In this band, red supergiants (RSG) should easily overcome NIR emission from an accretion disk (Copperwheat et al. 2005). Therefore, these stars were of particular interest in most of the surveys (e.g., Heida et al. 2014; López et al. 2017; King & Lasota 2020). Although blue supergiants were, at first, perceived as viable candidates for donors in ULXs because of their prevalence in star-forming regions, where most of the ULXs are being found, it was later realised that the optical companions might be outshone by the emission from an irradiated accretion disk (e.g., Sutton et al. 2014) unless the separation is very large (Copperwheat et al. 2007). This bias toward high-luminosity NIR companions might be the reason why the majority of the detected companion candidates are RSGs (e.g., Heida et al. 2019). This is further complicated by the fact that we cannot measure distances to ULXs and RSGs directly and the distance to the coinciding galaxy is used as a proxy.

Even if RSG donors form only a small fraction of the intrinsic ULX population, most of these binary companions cannot be Roche-lobe (RL) filling stars. For example, Wiktorowicz et al. (2017) estimated that only $<1\%$ of all ULXs can be accompanied by supergiants if RLOF accretion is concerned exclusively. In binaries containing a compact object and a RSG companion, the mass ratio is typically high ($q = M_{\text{don}}/M_{\text{acc}} > 3$), especially for a NS accretor, which makes the RLOF dynamically unstable (e.g., van den Heuvel et al. 2017) and leads to a common envelope phase (e.g., Ivanova et al. 2013).

One should stress, however, that $q > 3$ may not imply dynamical instability if the stellar envelope is radiative. In this case, which corresponds to the initial phase of Case B binary mass exchange, the MT rate occurs at the thermal (Kelvin–Helmholz) timescale (Kippenhahn & Weigert 1967; Kippenhahn et al. 1967) and is equal to

$$\dot{M} \equiv \frac{M_{\text{don},\star}}{t_{\text{KH}}} = 3.2 \times 10^{-8} \frac{R_{\text{don},\star} L_{\text{don},\star}}{M_{\text{don},\star}} M_{\odot} \text{ yr}^{-1}, \quad (1)$$

where $M_{\text{don},\star}$, $R_{\text{don},\star}$, and $L_{\text{don},\star}$ are the mass, radius and luminosity of the donor, and index \star designates solar units (Paczynski 1971). This transfer mechanism might power the brightest ULXs (Wiktorowicz et al. 2017). We note that some simulations predict a wider range of binary parameters that give stable mass transfer (Pavlovskii et al. 2017).

Previous theoretical studies mostly neglected a possibility that ULXs can be “fed” by stellar winds because, in general, stellar winds are fast and tenuous, so only a small fraction can reach the vicinity of the accretor (see e.g., Pakull et al. 2006; Copperwheat et al. 2007). However, RSGs undergo a significant mass loss in stellar wind, which can be slow in the vicinity of the donor, and can therefore provide a significant wind-fed mass transfer (MT) rate if the separation is small enough or if the wind is focused toward the accretor (El Mellah et al. 2019). The presence of an accretion disk in at least two wind-fed XRBs was inferred from spectroscopic observations and modeling (Vela X-1, Liao et al. 2020; and Cyg X-1, Zdziarski 2014).

Recently, Heida et al. (2019) suggested that the growing number of ULXs with RSG donor candidates prompts us to reevaluate the significance of wind-driven MT in the context of ULXs. However, to date, no general population studies of wind-fed ULXs have been done, even though at least one ULX was detected with a donor that is not filling its RL (e.g., M 101

⁹ The relevant accretion rate is that in the external part of the accretion flow where wind mass-loss is negligible.

ULX-1, Liu et al. 2013). The aim of this article is to tackle this problem. In particular, we will answer the following question: how important is the wind-fed accretion for ULX sources? Specifically, we perform a statistical analysis of binary evolution models in the context of recent observations to derive the number and properties of wind-fed ULXs. We focus on NS ULXs with RSG donors and progenitors of gravitational wave sources, such as GW170817.

2. Methods

In this section we will describe our adopted models (modes) of wind accretion. The inclusion of wind accretion in XRB models is the most significant difference to the previous population studies of ULXs. Bondi–Hoyle–Lyttleton (BHL) accretion is a standard scheme of wind mass accretion in *StarTrack* (Belczynski et al. 2008, 2020). Additionally, we adapt the wind RLOF (WRLOF) scheme, which was already used by Ikiewicz et al. (2019) to analyze the relation between SNIa and wide symbiotic stars.

The main source of uncertainty for accretion models is actually the origin of the wind mass-loss from the donor star. The standard model for stellar winds as implemented in *StarTrack* is described in Belczynski et al. (2010a). In short, we use the wind mass-loss prescriptions for OB stars based on observational data (Vink et al. 2001; Vink 2008). For Wolf-Rayet wind, the code accounts for clumping (Hamann & Koesterke 1998) and metallicity dependence (King & Lasota 2005). Wind mass-loss rates for luminous blue variable stars are calculated from $1.5 \times 10^{-4} (M/M_{\odot}) M_{\odot} \text{yr}^{-1}$ (Vink & de Koter 2002; Belczynski et al. 2010a). For low-mass stars, we follow the formalism of Hurley et al. (2000). This prescription is a minimal realistic one as far as the scarcity of the available observational data is concerned, but we note that the actual model realised in Nature may diverge from what we employed. This should be investigated by future observational campaigns.

2.1. Bondi–Hoyle–Lyttleton Accretion

In the BHL scheme (Hoyle & Lyttleton 1939; Bondi 1952, for a recent review see Edgar 2004), we assume that the accretor is engulfed by a steady and uniform (at least in the vicinity of the accretor) supersonic wind from a companion star with $v_{\text{wind}} \gg v_{\text{orb}}$, where v_{wind} is the wind velocity relative to the accretor and v_{orb} is the orbital velocity of the accretor relative to the mass losing star. We calculate the fraction of the wind mass-loss accreted by the compact body as (for derivation see Belczynski et al. 2008, Equation (39))

$$\beta_{\text{acc,BHL}} = \frac{\dot{M}_{\text{acc,BHL}}}{\dot{M}_{\text{don,wind}}} = \frac{1}{\sqrt{1-e^2}} \times \left(\frac{GM_{\text{acc}}}{v_{\text{wind}}^2} \right)^2 \frac{\alpha_{\text{wind}}}{2a^2} \left(1 + \left(\frac{v_{\text{orb}}}{v_{\text{wind}}} \right)^2 \right)^{-\frac{3}{2}}, \quad (2)$$

where $\dot{M}_{\text{acc,BHL}}$ is the orbit-averaged wind accretion rate, e is the eccentricity, G is the gravitational constant, M_{acc} is the accretor’s mass, a is the binary separation, and $\dot{M}_{\text{don,wind}}$ is the mass-loss rate in wind from the donor. α_{wind} is a numerical factor between 1 and 2 (Boffin & Jorissen 1988; Shima et al. 1985). Following Belczynski et al. (2008), we assume a conservative value of $\alpha_{\text{wind}} = 1.5$. We impose a limit of

$\dot{M}_{\text{acc,BHL}} \leq 0.8 \times \dot{M}_{\text{don,wind}}$ to avoid artificially high values resulting from orbital averaging. A formula similar to Equation (2) was first proposed by Bondi (1952), but later Shima et al. (1985) showed that an additional factor of ~ 2 makes the Bondi’s formalism fit their hydrodynamical simulations and agree with the earlier simplified prescription of Hoyle & Lyttleton (1939).

Here we make an optimistic assumption that all of the mass that is captured into the wake is consequently accreted, although only a fraction of this mass is expected to be accreted in a real situation (e.g., Edgar 2004). We also do not include any effects of orbital motion on the accretion flow, which could additionally decrease the accretion rate (e.g., Theuns et al. 1996). Consequently, the mass-accretion rate calculated through Equation (2) should be perceived as an approximate upper limit and our results should be seen as optimistic.

2.2. Wind RLOF

When the stellar wind is slow inside the donor’s RL, the assumption of wind isotropy may not be realistic because the accretor can gravitationally focus the wind toward the L1 point, thus imitating RLOF-like mode of accretion (including formation of an accretion disk). In such a case, one speaks about WRLOF. Mohamed & Podsiadlowski (2007) showed that it can provide much higher rates than BHL accretion in favourable circumstances. According to their simulations, which are limited to few special cases, WRLOF MT rate can be even 100 times higher than for BHL. The WRLOF has been already used to explain the observations of symbiotic stars (e.g., Mohamed & Podsiadlowski 2007; Ikiewicz et al. 2019), carbon-enhanced metal-poor stars (Abate et al. 2013). In particular, El Mellah et al. (2019) showed that wind-powered XRBs with supergiant donors can appear as ULXs in favourable conditions.

The MT may resemble the standard RLOF in detached binaries containing stars that have slow, dust-driven wind (Mohamed & Podsiadlowski 2007). The slow moving material fills the RL of the donor (stellar wind source), before being significantly accelerated by the radiation pressure and escaping preferentially through L1 point. Therefore, a significant fraction of the wind may be collimated toward the orbital plane and the accretor.

The formalism for WRLOF used in the present study, which we describe below, was first developed by Abate et al. (2013). Motivated by numerical simulations (e.g., Mohamed 2010), we assume that the collimation of stellar wind toward the orbital plane and the accretor is significant when the radius where the stellar wind accelerated by the radiation pressure reaches the escape velocity (R_d) is comparable to or larger than the RL radius. Assuming $R_d \gg R_{\text{don}}$, the former can be approximated as (Höfner 2007):

$$R_d = \frac{1}{2} R_{\text{don}} \left(\frac{T_{\text{eff}}}{T_{\text{cond}}} \right)^{\frac{4p}{2}}, \quad (3)$$

where R_{don} is the donor’s radius, T_{eff} the donor’s effective temperature, T_{cond} is the condensation temperature of the dust, and p is a parameter. Although T_{cond} and p depend on the chemical composition, we assume the values of $T_{\text{cond}} = 1500 \text{ K}$ and $p = 1$, which are consistent with properties of carbon-rich dust (e.g., Höfner 2007).

Table 1
Number of ULXs for a Fiducial Galaxy

Model	Constant SF			Burst SF (100 Myr ago)			Burst SF (2 Gyr ago)		
	RLOF	WIND	f_{WRLOF}	RLOF	WIND	f_{WRLOF}	RLOF	WIND	f_{WRLOF}
All Companions									
WM0	2.4×10^1	2.3×10^1	...	6.8×10^2	2.1×10^3	...	2.2×10^1	3.7×10^{-2}	...
WM8	2.4×10^1	3.7×10^1	42.50%	6.8×10^2	2.9×10^3	33.63%	2.2×10^1	1.7×10^{-2}	100.00%
WM+	2.4×10^1	1.9×10^2	97.24%	6.8×10^2	1.8×10^4	97.96%	2.2×10^1	1.7×10^{-2}	100.00%
Supergiant Companions									
WM0	5.3×10^{-2}	2.0×10^1	...	5.2	1.8×10^3
WM8	5.3×10^{-2}	3.3×10^1	44.45%	5.2	2.7×10^3	36.08%
WM+	5.3×10^{-2}	1.8×10^2	98.60%	5.2	1.8×10^4	99.33%
RSG Companions									
WM0	1.6×10^{-5}	2.0×10^1	...	1.6×10^{-3}	1.8×10^3
WM8	1.6×10^{-5}	3.2×10^1	43.51%	1.6×10^{-3}	2.6×10^3	35.57%
WM+	1.6×10^{-5}	1.8×10^2	98.56%	1.6×10^{-3}	1.7×10^4	99.32%

Note. Predicted numbers of ULXs powered by Roche lobe overflow (RLOF) and wind accretion (WIND) in a fiducial galaxy (see text for details). f_{WRLOF} gives a fraction of wind-fed ULXs in which MT occurs through wind RLOF mode (Section 2.2). Models presented are: WM0 in which only BHL accretion mode is possible, WM8 in which WRLOF accretion mode possible, but limited to donors lighter than $8 M_{\odot}$, and WM+ in which WRLOF accretion mode possible for donors of all masses. Additionally, supergiant and RSG donors are shown separately. Supergiant companions are defined as post-MS stars with luminosity $L > 15,000 L_{\odot}$ and surface gravity $\log g < 2$, whereas RSGs, a subpopulation of supergiants, additionally have effective surface temperatures lower than 4kK. Results for three reference SFHs are presented: constant through 10 Gyr and burst-like with a duration of 100 Myr which started 100 Myr or 2 Gyr ago. Zeros are marked with “-” for clarity.

The stellar-wind fraction reaching the accretor is calculated as (Abate et al. 2013, see Equation (9) therein):

$$\beta_{\text{acc,WRLOF}} = \min \left\{ \left(\frac{q}{0.6} \right)^2 [c_1 x^2 + c_2 x + c_3], \beta_{\text{acc,max}} \right\}, \quad (4)$$

where $x = R_d/R_{\text{RL,don}}$, $R_{\text{RL,don}}$ is the RL radius of the donor, $c_1 = -0.284$, $c_2 = 0.918$, and $c_3 = -0.234$. $c_1 x^2 + c_2 x + c_3$ is a fit to the results of Mohamed (2010) made for $q = 0.6$, q being the mass ratio (donor mass over accretor mass). $(q/0.6)^2$ is the scaling proposed by Abate et al. (2013) to account for the influence of the mass ratio on the MT rate. $\beta_{\text{acc,max}} = 0.5$ is the highest value of β_{acc} obtained by Mohamed (2010), which we use as the limit for all values of q . If the MT rate calculated for the WRLOF is higher than the BHL rate, then we assume that MT occurs through WRLOF mode. In the opposite case, we assume that it occurs through BHL mode.

We are aware that the simulation of Mohamed (2010) and calculations by Abate et al. (2013) were performed for a narrow region of the parameter space (viz. specific values of accretor and donor masses). Nonetheless, we extended the applicability of their results to suit the needs of population synthesis calculations. In our reference model (WM8), we allow for the WRLOF MT mode only from donors less massive than $8 M_{\odot}$, which is just the maximal mass to which simulations were performed in Mohamed (2010). For comparison we provide also the results for two other models. In the WM0 model the WRLOF MT is not possible and all wind-fed systems transfer mass using BHL mode. Meanwhile, in the model WM+, WRLOF MT is allowed for all donors irrespective of their mass. These two variations may be seen as extreme cases as far as the importance of WRLOF is concerned.

2.3. Simulations

To obtain statistically significant comparison of observational data on ULX sources with models of wind-fed accretion, we utilized the population synthesis code `StarTrack` (Belczynski et al. 2008, 2020). In a previous paper

(Wiktorowicz et al. 2019a), we analyzed the observed population of ULXs but focused on the RLOF systems only. In the current work, ULXs in which accretion occurs via RLOF serve as a reference point. The beaming (i.e., anisotropic emission of radiation) can be present in ULXs in general (e.g., Wiktorowicz et al. 2019a) and specifically in PULXs (King & Lasota 2020). Therefore, we include these effects in our analysis of wind-fed ULXs, as was previously done for the population of RLOF ULXs in Wiktorowicz et al. (2019a).

To compare the theoretical binary evolution models and observational data, we calculate the predicted number of RLOF-fed and wind-fed ULXs, for a fiducial galaxy that resembles the Milky Way. Specifically, we assumed the total stellar mass to be $M_{\text{tot}} = 6.08 \times 10^{10} M_{\odot}$ (Licquia & Newman 2015), a uniform metallicity distribution ($Z = Z_{\odot} = 0.02$) and constant star formation rate (SFR) throughout the last 10 Gyr equal to $6.08 M_{\odot} \text{ yr}^{-1}$. We also present results for burst-like star formation episodes ($\Delta t = 100$ Myr; $\text{SFR} = 608 M_{\odot} \text{ yr}^{-1}$) for comparison at two moments: 100 Myr and 2 Gyr after the commencement of star formation (i.e., right after and 1.9 Gyr after the star formation ceases), which correspond to young and old stellar populations, respectively. Due to the inaccuracies of evolutionary models and sparse observational data, a more-detailed Galactic model is not necessary in the context of this work.

3. Results

3.1. Observable Sample

Table 1 presents the abundance of ULXs (both RLOF- and wind-fed) in our results. Although these numbers are rather optimistic due to favorable assumptions, particularly the high recent SFR used in the simulations and the omission of interstellar absorption, they show that the inclusion of wind-fed sources in ULX populations studies is necessary. Wind-fed ULXs may not only represent a significant fraction of the ULX population (e.g., 49%–89% for constant star formation history) but, in favorable conditions (e.g., very young stellar environments), may also be its dominant component. We note that

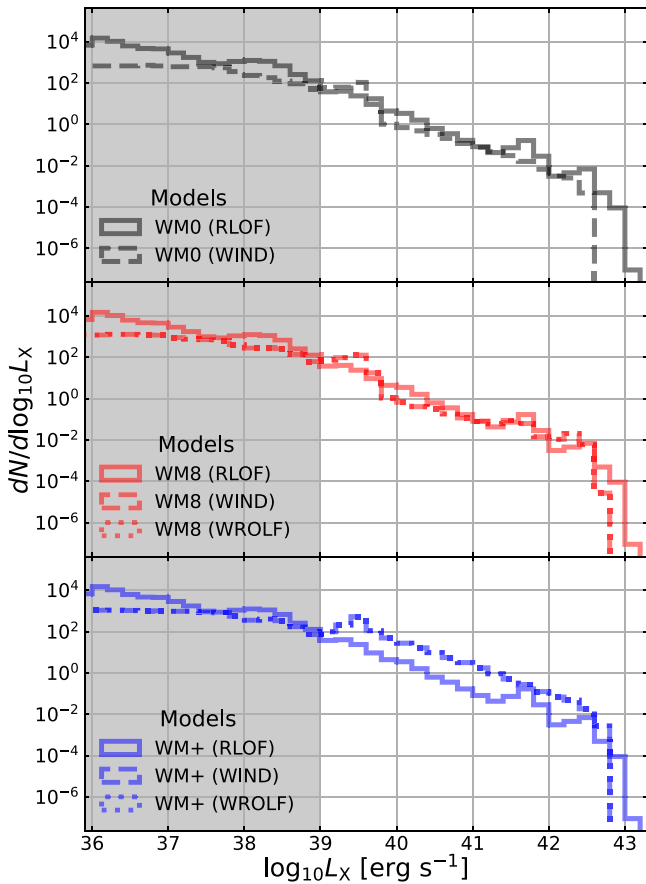


Figure 1. Distributions of X-ray luminosity (L_X) of ULXs for the various models tested in this study (see text for details). The shaded area presents the extension for regular XRBs ($L_X < 10^{39} \text{ erg s}^{-1}$), but is not a part of this study. Designations in parenthesis mark the ULX subpopulations: RLOF-powered by the RLOF accretion mode; WIND-powered by wind-fed accretion (both WRLOF and BHL modes); WRLOF-powered by WRLOF accretion mode only.

these results may change significantly if the actual wind-emission model from massive stars differs from that used in the current study.

The population of ULXs is dominated by sources with low luminosities ($\lesssim 3 \times 10^{39} \text{ erg s}^{-1}$) both for RLOF and wind-powered sources (Figure 1). These are mainly BH ULXs emitting isotropically and mildly-beamed (beaming factor¹⁰ $b \gtrsim 0.2$) NS ULXs. In the case of wind-fed ULXs, both modes (viz. BHL and WRLOF) are possible. As far as the most luminous sources are concerned, the highest luminosities (up to $\sim 10^{43} \text{ erg s}^{-1}$) are obtained for binaries consisting of a NS with a Helium rich donor or a BH with a HG donor (see also Wiktorowicz et al. 2015). In the case of wind-fed sources, this highly luminous group is composed of ULXs with BH accretors transferring mass through the WRLOF mode exclusively. In all cases, we assume that the beaming is saturated at $b \approx b_{\min} = 3.2 \times 10^{-3}$ (Lasota et al. 2016; Wiktorowicz et al. 2017). We note, that no ULXs have been observed with luminosities much above $\sim 10^{42} \text{ erg s}^{-1}$ and some ULXs with luminosities above $\sim 10^{41} \text{ erg s}^{-1}$ might actually contain intermediate-mass BHs (e.g., Greene et al.

2020), which are not included in our study. Nonetheless, although these luminous stellar-mass ULXs are rare (we predict $\sim 10^{-7}$ per Milky Way equivalent galaxy), they may exist undetected in distant galaxies. King (2009) suggested that such highly beamed and apparently luminous sources may mimic distant AGNs acting as “pseudoblazars.”

The wind-fed ULXs can reach similar luminosities as RLOF systems, despite the large fraction of mass being lost from the system (e.g., Mohamed 2010, obtained that no more than 50% of wind is accreted). This is possible because the wind-fed systems do not suffer from dynamical instability when the mass ratio is high ($\gtrsim 3$), even when their envelopes are convective (van den Heuvel et al. 2017, and references therein), and they can have very massive donors. Consequently, the progenitors of wind-fed ULXs are typically more massive on the ZAMS and have larger separations to accommodate expanding stars (Figure 2).

The RLOF-powered ULXs typically have much longer duration of the emission phase ($> 5 \text{ Myr}$) than wind-fed systems ($\sim 1 \text{ Myr}$ for WRLOF and $\sim 0.1 \text{ Myr}$ for BHL; see Figure 3). The donors in wind-fed systems are typically massive stars (Figure 7) in a short-lived supergiant phase (e.g., $\sim 1.5 \text{ Myr}$ for $5 M_{\odot}$ asymptotic giant branch star (AGB) or $\sim 0.1 \text{ Myr}$ for $10 M_{\odot}$ AGB star) when their wind is relatively slow and dense. Meanwhile, RLOF accretion may give high MT rates even for low-mass companions at the end of MS phase (e.g., Wiktorowicz et al. 2017). Low-mass stars have significantly longer life spans than their heavier cousins. Therefore, they potentially have longer MT phases and less often enter dynamical-time MT when their RL is filled. We note that it is only possible for the donor in a RLOF-powered ULX to fill its RL immediately after the compact object formation as a result of favorably directed natal kick in rare situations (see e.g., Maxted et al. 2020), so that its MT phase can be the longest possible. In a typical case, the RL is filled only after the star expands as a result of nuclear evolution, which is typically shortly ($\lesssim 100 \text{ Myr}$) before TAMS.

RLOF ULXs are typically associated with low- and medium-mass donors ($\lesssim 10 M_{\odot}$), whereas wind-fed ones typically have massive donors ($\gtrsim 10 M_{\odot}$; Figure 7). Although low-mass stars are more abundant among primaries due to the shape of the initial mass function ($\Gamma < 0$), flat initial mass ratio distribution makes massive companions more prevalent among NS/BH progenitors (Figure 2; see also Wiktorowicz et al. 2019b). This situation favors wind-fed ULXs. The higher the mass of a star, the stronger is the mass loss in stellar wind for a particular evolutionary phase. This makes a binary with compact object progenitor and massive secondary a perfect predecessor of a wind-fed ULX. Moreover, when a massive star fills its RL after the primary forms a compact object, the mass ratio may be too high to provide a stable RLOF MT and instead a CE occurs and this bars the formation of a ULX. We note that ULXs powered by RLOF MT have been discussed thoroughly in previous studies (e.g., Wiktorowicz et al. 2017).

3.2. Typical Evolution

Wind-fed ULXs are expected to comprise a large fraction (up to $\sim 96\%$) of ULXs in star-forming environments, but practically disappear ($< 1\%$) in old environments (Table 1). These systems may contain either a BH or a NS accretor, and they may be powered by WRLOF or BHL wind accretion mode. However, NS accreting through WRLOF mode

¹⁰ The beaming factor b is the ratio of the solid angle of emission and the whole sphere. In this study we assume $b = \min(1, 73 / (\dot{M} / \dot{M}_{\text{Edd}})^2)$, where \dot{M} and \dot{M}_{Edd} are the actual and the Eddington accretion rates, respectively (King 2009; Wiktorowicz et al. 2019a).

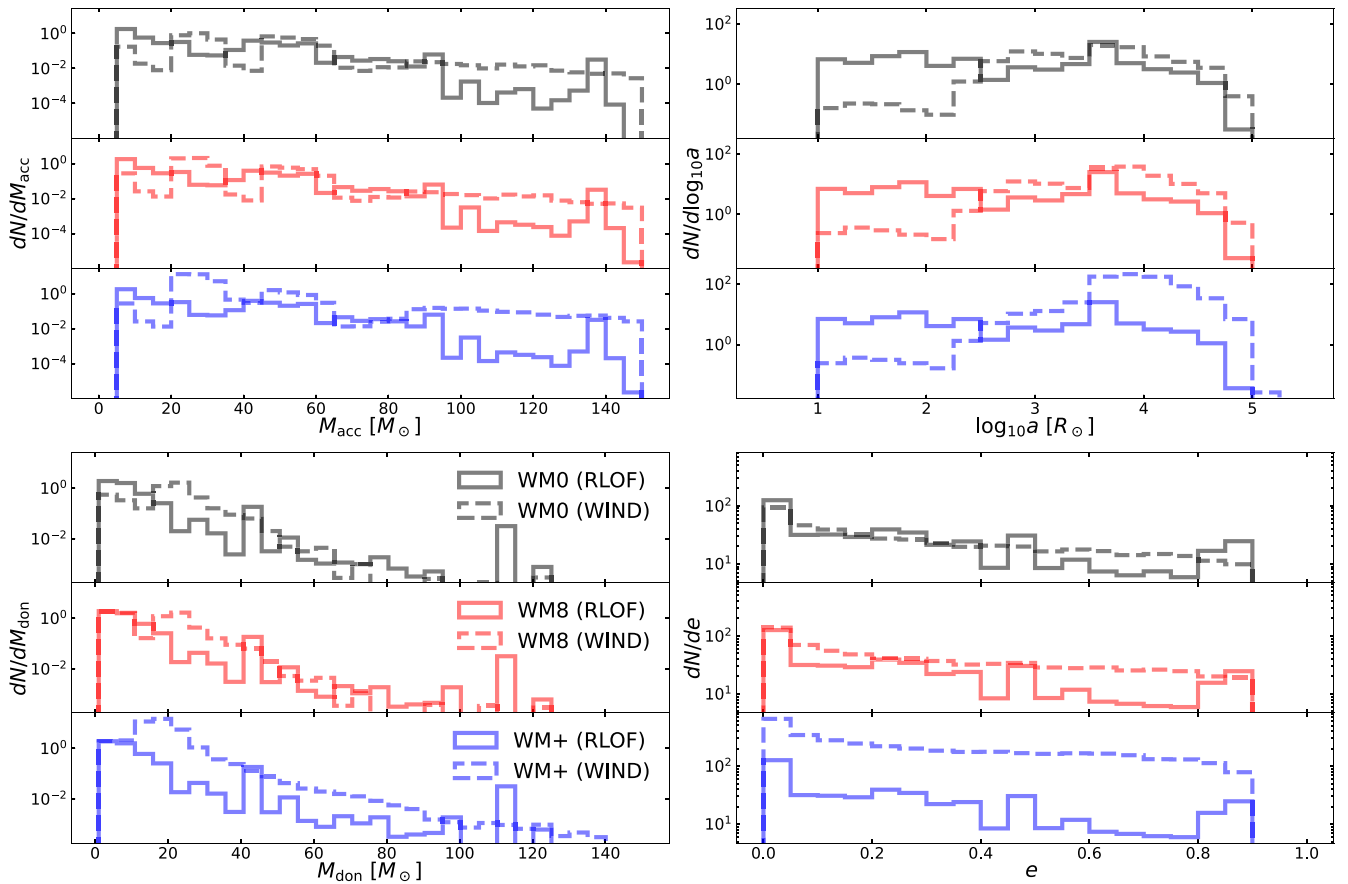


Figure 2. Initial distributions of parameters for ULX progenitors with division on different tested models and accretion modes (see caption of Figure 1). Parameters are: M_{acc} —accretor mass; M_{don} —donor mass; a —separation; e —eccentricity.

dominates the population in older environments ($\gtrsim 1$ Gyr after the end of star formation). In this section, we compare various evolutionary routes leading to the formation of wind-fed ULXs and their posterior evolution.

The most common wind-fed ULXs are those with NS accretors and MT occurring through the WRLOF mode. Donors in these systems are typically low-mass ($0.7\text{--}2.6 M_{\odot}$) AGB stars. In a typical case (Figure 4, upper plot), the binary on ZAMS composes of a $7.48 M_{\odot}$ primary and a $2.28 M_{\odot}$ secondary on a medium-size orbit of $\sim 3200 R_{\odot}$ with moderate eccentricity ($e \approx 0.2$). The primary evolves and becomes an AGB star at the age of 48 Myr. The stellar wind leads to a significant mass loss, part of which is captured by the secondary. Finally, the primary becomes a $1.36 M_{\odot}$ ONe white dwarf (WD), whereas the secondary grows to $\sim 3 M_{\odot}$ while still being on the MS. After 460 Myr, the secondary evolves off the MS and becomes an AGB star, which results in a significant rise in the rate of mass loss in stellar wind. The WD captures a fraction of the wind, which allows it to grow to $1.38 M_{\odot}$, when the accretion induced collapse transforms it into a $1.26 M_{\odot}$ NS. The secondary remains an AGB star for the next 0.7 Myr, while the mass loss increase and in a short time reaches $\sim 10^{-6} M_{\odot} \text{ yr}^{-1}$ out of which 37% is captured into the primary disk. This marks the beginning of the ULX phase that lasts for 100 kyr and the luminosity reaches $\sim 4 \times 10^{41} \text{ erg s}^{-1}$. Afterwards, the secondary becomes a $0.75 M_{\odot}$ CO WD.

The progenitors of NS ULXs powered through the BHL mode require heavier companions ($1.2\text{--}2.4 M_{\odot}$) and larger initial separations. In a typical case (Figure 4, lower plot), the

system initially consists of a $7.1 M_{\odot}$ primary and $4.1 M_{\odot}$ secondary on a wide eccentric orbit ($a \approx 8700 R_{\odot}$; $e \approx 0.46$). The primary, while ascending the AGB, loses most of its mass and at the age of 54 Myr becomes an ONe WD. As a result of mass accretion, the secondary grows to $\sim 5.5 M_{\odot}$ and after 80 Myr becomes an AGB star. In one Myr, it loses nearly $2 M_{\odot}$ of its mass, due to strong stellar wind, a fraction of which is captured by the WD, which increases its mass to $1.38 M_{\odot}$ when the electron-capture SN results in the formation of a NS. In such an accretion induced collapse, the natal kick is expected to be low, which allows the wide binary with a separation of $18,000 R_{\odot}$ and moderate eccentricity of $e \approx 0.27$ to survive. Such a large separation makes WRLOF ineffective and the MT occurs through the BHL mode. Although the fraction of the wind being accreted is small ($\sim 2\%$), the strong stellar wind ($6.5 \times 10^{-5} M_{\odot} \text{ yr}^{-1}$) makes the effective MT quite high ($1.5 \times 10^{-6} M_{\odot} \text{ yr}^{-1}$), comparable to that in typical NS ULX powered through the WRLOF mode (see paragraph above). The luminosity reaches 3.5×10^{40} for a brief moment, but within 3 kyr the system dims and becomes a regular XRB. After 100 kyr, the secondary becomes a WD with a mass of $\sim 1.06 M_{\odot}$.

We note that AGB stars with mass-loss rates as in the above examples are observed in the Large Magellanic Cloud (e.g., Höfner & Olofsson 2018). Therefore, the accretion efficiencies in WRLOF mode that are necessary to power a ULX for the observed mass-loss rates are within the model range (i.e., ≤ 0.5). Concerning the BHL accretion mode, we may estimate the accretion radius as $R_{\text{acc}} = 2GM_{\text{acc}}/v_{\text{inf}}^2$, where G is the

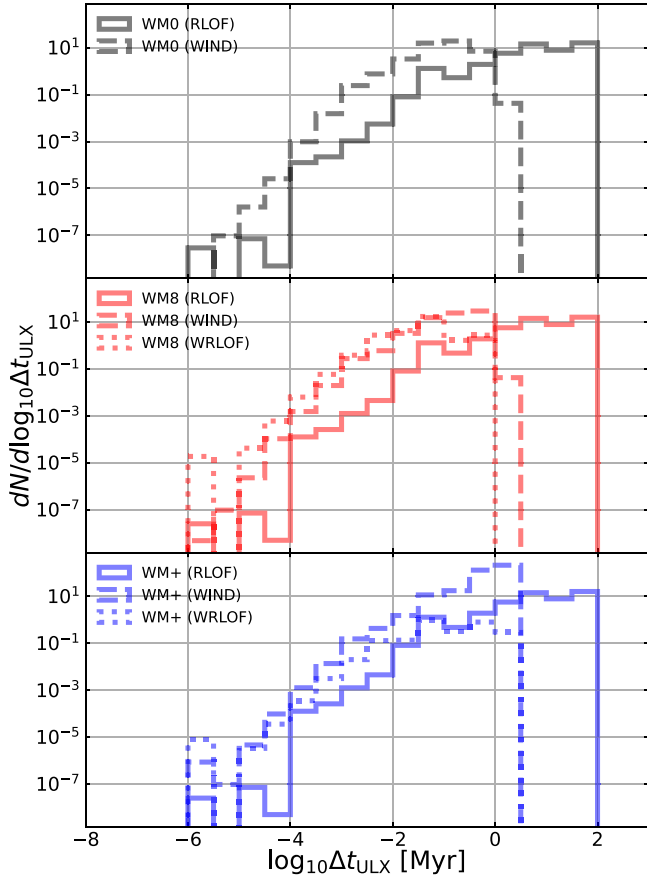


Figure 3. Distribution of the ULX phase total duration times (Δt_{ULX}) with a division on different models and accretion modes (see the caption of Figure 1). The durations are combined when a system has more than one ULX phase during its evolution.

gravitational constant and v_{inf} is the terminal wind velocity (e.g., Edgar 2004). The fraction of accreted wind may be further estimated as the fraction of the wind that falls within the accretion radius:

$$f_{\text{acc}} = 0.5 \sin R_{\text{acc}}/a \approx 0.095 (M/M_{\odot})(v_{\text{inf}}/10 \text{ km s}^{-1})^{-2}(a/20,000 R_{\odot})^{-1}$$

where $v_{\text{inf}} \approx 10 \text{ km s}^{-1}$ is the typical value for AGB stars (e.g., Höfner & Olofsson 2018). Although these estimations are very rough (see Section 4.2), they show that the MT rates in the typical routes are feasible.

The companions in wind-powered BH ULXs are (in general) more massive than in NS ULXs. This results from the fact that heavier primaries (BH progenitors) are typically accompanied by heavier secondaries ($\gtrsim 10 M_{\odot}$) on the ZAMS (e.g., Wiktorowicz et al. 2019b). For BH ULXs, in which the MT occurs through WRLOF mode, the typical companion mass is 5–7 M_{\odot} , whereas a BH is typically ~ 8 –9 M_{\odot} . In a typical evolution leading to the formation of such a system (Figure 5, upper plot), the primary on ZAMS is 26.1 M_{\odot} , whereas the secondary is 6.65 M_{\odot} , and the separation is 12,000 R_{\odot} with significant eccentricity $e \approx 0.51$. The primary evolves more quickly and after 6.7 Myr becomes a CHeB star. A high wind mass-loss starts that decreases the star’s mass to 9.2 M_{\odot} in just 700 kyr. A fraction of this mass is accreted by the secondary, which allows it to retain its initial mass of $\sim 6.7 M_{\odot}$ despite loses in stellar wind. Shortly after, the primary forms a 8.37 M_{\odot} BH. Meanwhile, the separation increases to 20,000 R_{\odot}

NS ULX WRLOF accretion mode						
age [Myr]	NS ULX WRLOF accretion mode		phase	$M_a[M_{\odot}]$	$M_b[M_{\odot}]$	
0	MS	• MS	ZAMS	7.48	2.28	
	$a \approx 3200 R_{\odot}; e \approx 0.20$					
517	NS	•	AGB	1.26	2.85	
	$a \approx 4,900 R_{\odot}; e \approx 0.03$					
517	NS	•	WRLOF	1.27	2.67 (0.75)	
	$a \approx 5,100 R_{\odot}; e \approx 0.03$					
518	NS	•	WD	1.27	0.75	
	$a \approx 10,000 R_{\odot}; e \approx 0.03$					
NS ULX BHL accretion mode						
age [Myr]	NS ULX BHL accretion mode		phase	$M_a[M_{\odot}]$	$M_b[M_{\odot}]$	
0	MS	• MS	ZAMS	7.10	4.11	
	$a \approx 8,700 R_{\odot}; e \approx 0.46$					
131	NS	•	AGB	1.26	3.74	
	$a \approx 18,000 R_{\odot}; e \approx 0.27$					
131	NS	•	BHL	1.26	3.74 (1.06)	
	$a \approx 40,000 R_{\odot}; e \approx 0.27$					
131	NS	•	WD	1.26	1.06	
	$a \approx 40,000 R_{\odot}; e \approx 0.27$					

Figure 4. Symbolical representation of a typical system evolution leading to the formation of wind-fed NS ULXs. Upper/Lower plots show routes with WRLOF/BHL accretion mode. The columns represent the age of the system, scheme of the system (not to scale), evolutionary phase, and masses of the primary and secondary. The binary evolution phases are as follows: ZAMS—zero age main sequence; AIC—accretion induced collapse; WRLOF—phase of wind accretion through WRLOF mode; BHL—phase of wind accretion through Bondi–Hoyle–Lyttleton mode; WD—white dwarf formation. Additionally, the schemes present separations (a), eccentricities (e), and stellar evolutionary phases: MS—main sequence; AGB—asymptotic giant branch; NS—neutron star; WD—white dwarf.

and the eccentricity changes to 0.33. The secondary needs more than 50 Myr to evolve off the MS and become an AGB star, when its wind mass loss grows significantly to 4.6×10^{-7} . The wind is still slow inside the RL. Therefore, a large fraction ($\sim 50\%$) is gravitationally collimated toward the L1 point and feeds the accretion disk of the primary. For 500 kyr, the MT through WRLOF mode is high enough to power a ULX with the peak luminosity reaching $\sim 10^{42} \text{ erg s}^{-1}$. Afterwards, the secondary becomes a CO WD with a mass of 1.23 M_{\odot} .

The evolution leading to the formation of BH ULXs powered by BHL accretion (Figure 5, lower plot) differs significantly from the cases described above. The companions are significantly more massive, 9–12 M_{\odot} , thus the WRLOF can operate only in WM+ model, which allows for wind collimation from donors with masses above 8 M_{\odot} . On the ZAMS, the binary consists of a 23.8 M_{\odot} primary and a 19.7 M_{\odot} secondary on an orbit of 5400 R_{\odot} , which is nearly circular ($e \approx 0.02$). The primary evolves and in 7.3 Myr becomes a CHeB star, which commences a significant mass loss in stellar wind. Within 800 kyr, the star loses more than half of its mass in stellar wind and becomes a 8.34 M_{\odot} BHs. The secondary evolves and at the age of ~ 10 Myr, as a CHeB star, provides a MT rate of $1.2 \times 10^{-5} M_{\odot} \text{ yr}^{-1}$, out of which $\sim 2\%$ reaches the vicinity of the accretor. It is high enough to power an isotropic ULX ($L_X \approx (2\text{--}3) \times 10^{39} \text{ erg s}^{-1}$) for ~ 100 kyr. Meanwhile,

age [Myr]	BH ULX WRLOF accretion mode		phase	$M_a[M_\odot]$	$M_b[M_\odot]$
0	MS 	 MS	ZAMS	26.1	6.65
	$a \approx 12,000 R_\odot; e \approx 0.51$				
7.5	BH 	 MS	SN	8.37	6.68
	$a \approx 20,000 R_\odot; e \approx 0.33$				
62	BH 	 AGB	WRLOF	8.38 (8.42)	6.47 (1.24)
	$a \approx 20,000 R_\odot; e \approx 0.33$				
62	BH 	 WD	WD	8.42	1.23
	$a \approx 31,000 R_\odot; e \approx 0.33$				
age [Myr]	BH ULX BHL accretion mode		phase	$M_a[M_\odot]$	$M_b[M_\odot]$
0	MS 	 MS	ZAMS	23.8	19.7
	$a \approx 5,400 R_\odot; e \approx 0.02$				
8.1	BH 	 MS	SN	8.34	19.9
	$a \approx 7,700 R_\odot; e \approx 0.00$				
10	BH 	 CheB/AGB	BHL	8.37	11.2 (7.83)
	$a \approx 9,600 R_\odot; e \approx 0.00$				
10	BH 	disruption  NS	SN	8.38	1.74

Figure 5. Same as Figure 4, but for ULXs with BH accretors. Additional abbreviations (not present in Figure 4) for binary evolution include: SN–supernova (i.e., formation of the compact object); whereas for stellar evolution: BH–black hole; CheB–core Helium burning.

the secondary evolves into an AGB star and the luminosity of the ULX increases to reach $\sim 10^{42}$ erg s $^{-1}$. After that time, the secondary, having a mass of $7.8 M_\odot$, undergoes a SN and becomes a NS. However, the NS’s natal kick on such a wide orbit ($a \approx 13,000 R_\odot$) results in a binary disruption. We note that the accretion mode in this scenario is forced by the limit on the maximal mass of donor as $8 M_\odot$ in WRLOF mode for the reference mode. In the WM+ model, this ULXs will transfer mass through WRLOF mode but the peak luminosity will be similar.

A few ULXs evolve through both the RLOF-powered phase and wind-powered phases. This situation occurs for 4% of RLOF ULXs and 5% of wind-fed ULXs (1%/8% in the case of WM0/+ models, respectively) predicted to be observed currently in the modeled galaxy. In a typical case (Figure 6), such a binary on the ZAMS is composed of a $29.9 M_\odot$ primary and $3.56 M_\odot$ secondary, whereas the separation and eccentricity are $4400 R_\odot$ and 0.10, respectively. The primary evolves much more quickly and becomes a CheB star. The mass loss in the stellar wind removes most of the hydrogen envelope, so when the star fills its RL at the age of 6.5 Myr, the companion easily rejects the CE and the separation shrinks to $100 R_\odot$. The primary evolves as a helium star for 200 kyr and forms a $8.45 M_\odot$ BH. The orbit now is close enough for the secondary expanding as a RG to fill its RL and start a RLOF, which is strong enough to power a ULX and lasts for 400 kyr with a luminosity of approximately 6×10^{39} erg s $^{-1}$. The secondary detaches as the separation grows to $280 R_\odot$. Its RL is filled again when the star ascends the AGB. The star detaches when the separation grows to $1,200 R_\odot$, but still nearly fills its RL. This results in significant MT rate through WRLOF mode that

age [Myr]	BH ULX RLOF+BHL accretion mode		phase	$M_a[M_\odot]$	$M_b[M_\odot]$
0	MS 	 MS	ZAMS	29.9	3.56
	$a \approx 4,400 R_\odot; e \approx 0.10$				
6.7	BH 	 MS	SN	8.45	3.59
	$a \approx 120 R_\odot; e \approx 0.01$				
240	BH 	 RG	RLOF	8.45 (8.59)	3.59 (0.96)
	$a \approx 120 R_\odot; e \approx 0.00$				
290	BH 	 AGB	BHL	8.59 (8.60)	0.96 (0.81)
	$a \approx 1,200 R_\odot; e \approx 0.00$				
290	BH 	 WD	WD	8.60	0.79
	$a \approx 1,700 R_\odot; e \approx 0.00$				

Figure 6. Same as Figure 4, but for a ULX that is powered first by RLOF accretion and later by wind accretion. Additional abbreviations (not present in Figures 4 and 5) for the binary evolution are: RLOF–Roche-lobe overflow; and for stellar evolution: RG–red giant.

powers a ULX for 100 kyr with a luminosity of $\sim 3 \times 10^{39}$ erg s $^{-1}$. Afterwards, the secondary forms a $0.79 M_\odot$ WD.

3.3. Donors

Figure 7 presents the parameter distributions of donors in the sample of wind-fed ULXs. Donors in RLOF ULXs were thoroughly investigated in our previous papers (e.g., Wiktorowicz et al. 2017) and are provided here only for reference.

The masses of the donors in wind-fed systems are on average larger than in RLOF-fed ones and reach $30 M_\odot$ for WM0/8 models, or $\sim 70 M_\odot$ for WM+ model. Wind-fed accretion does not suffer from dynamical instability for high mass-ratio systems, which is the case of RLOF stars with convective envelopes, and allows for $q \gtrsim 3$. Meanwhile, the heavier the star, the shorter is its lifetime. This significantly limits the estimated number of ULXs with most massive donors and localizes them in star-forming regions or their immediate vicinity.

The evolutionary stage of wind-feeding donors is markedly different from those in RLOF ULXs, which are predominantly MS and He-rich stars. In wind-fed ULXs these are mostly CheB and AGB stars that have significantly expanded due to nuclear evolution, and produce dense and slow stellar wind. Being more massive, donors in wind-fed systems are also on average much younger than in RLOF ULXs. However, those in orbit with NSs may be much older and the ULX phase can occur as late as >1 Gyr after the ZAMS. We note that in a typical situation, the secondary becomes rejuvenated while accreting from stellar wind blown out from the evolving primary.

Donors in wind-fed ULXs are also more luminous than those in RLOF systems, mainly because of their higher masses and advanced evolutionary phase, with luminosities reaching $\sim 10^6 L_\odot$. These luminosities should be easily detectable at extragalactic distances, where the majority of ULXs are observed, and agrees with the fact that most of the donor candidates in ULXs are RSGs (Heida et al. 2019).

RSG donors are a minority in studies of ULX populations (e.g., $\lesssim 1\%$ in Wiktorowicz et al. 2017), as we show also in this

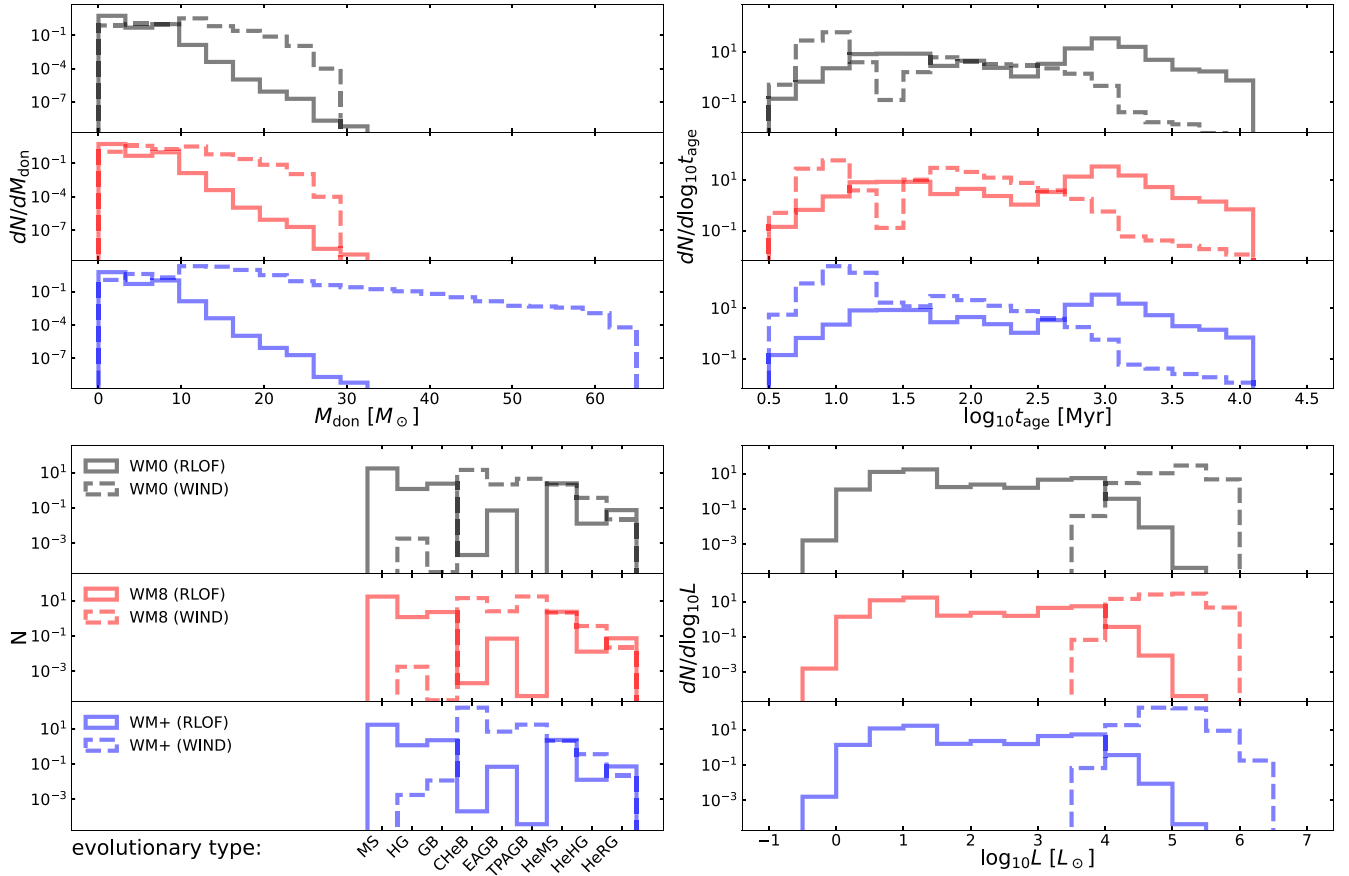


Figure 7. Distributions of ULX donor parameters: mass (M_{comp} , upper left-hand panel), age since ZAMS at the moment of observation (t_{age} , upper right-hand panel), evolutionary type (lower left-hand panel), and bolometric luminosity (L , lower right-hand panel). The maximum age of the ULXs was limited to 10 Gyr due to the duration of the simulation. Model names and accretion modes are defined in caption to Figure 1. Evolutionary types are: MS—main sequence; HG—Hertzsprung gap; RG—red giant; CHeB—Core Helium burning; EAGB—early asymptotic giant branch; TPAGB—thermal pulsing asymptotic giant branch; HeMS—Helium main sequence; HeHG—Helium Hertzsprung gap; HeRG—Helium red giant.

Table 2
Double Compact Object Progenitors Among ULXs

Model	MT Mode		All	DCO	mDCO	WRLOF DCO
WM0	RLOF	all	2.4×10^1	$7.2 \times 10^{-3}\%$	$1.1 \times 10^{-3}\%$...
		RSG	$6.8 \times 10^{-5}\%$	$1.7 \times 10^{-5}\%$
	WIND	all	2.3×10^1	46%	6.0%	...
WM8	RLOF	all	2.4×10^1	$7.2 \times 10^{-3}\%$	$1.1 \times 10^{-3}\%$...
		RSG	$6.8 \times 10^{-5}\%$	$1.7 \times 10^{-5}\%$
	WIND	all	3.7×10^1	32%	3.8%	3.2%
WM+	RLOF	all	2.4×10^1	$7.2 \times 10^{-3}\%$	$1.1 \times 10^{-3}\%$...
		RSG	$6.8 \times 10^{-5}\%$	$1.7 \times 10^{-5}\%$
	WIND	all	1.9×10^2	15%	0.75%	14%
		RSG	95%	14%	...	14%

Note. Predicted number of all ULXs for the tested models and accretion modes (see caption of Table 1) with fractions of this number that fall into different categories: All—all systems; DCO—ULXs that are DCO progenitors; mDCO—ULXs that are progenitors of merging DCOs; WRLOF DCO—ULXs that transfer mass through WRLOF mode and are DCO progenitors. Calculated for a Milky Way-like galaxy with constant star formation history. Rows labeled “RSG” present the subpopulation of ULXs with RSG donors. There are no ULXs that are progenitors or merging DCOs and transfer mass through WRLOF mode. Zeros are marked as “-” for clarity.

study ($\sim 6.8 \times 10^{-5}\%$). This did not produce a conflict with observations because donor candidates were only detected in a handful of ULXs and the observations were strongly biased toward detection of NIR objects. Additionally, ULXs are predominantly extragalactic objects, so low-mass, and therefore dim, stars, which theoretically dominate donors in RLOF-fed ULXs (e.g., Wiktorowicz et al. 2017), are naturally excluded

from detection. However, our study of wind-fed ULXs shows that in reality RSG might compose a significant fraction of ULXs, and in particular dominate those which are wind-fed ($\gtrsim 88\%$; see Table 2). Moreover, $\gtrsim 36\%$ of them may transfer mass through the WRLOF mode. Only in old stellar environments ($t_{\text{age}} \gtrsim 1$ Gyr) does the fraction of RSGs among ULXs peter out (Table 1) due to their short lifetimes. None of

the ULXs with RSG donors will evolve into a merging DCO (Section 3.4) and will instead typically form wide systems that are composed of a compact object and a carbon-oxygen WD.

According to our results, RSGs are expected to dominate the populations of wind-fed ULXs. This abundance of RSGs in our sample of synthetic ULXs suggests that the apparent connection between ULXs and RSGs in the observational data might be real.

3.4. Double Compact Object Progenitors

ULXs are among the potential double compact object (DCO) progenitors (e.g., Mondal et al. 2020). Heida et al. (2019) suggested that ULXs harboring RSGs, thus massive stars, are especially good candidates. However, as we have shown in Section 3.2, the majority of ULXs with RSG donors (and wind-fed ULXs in general) are expected to form either wide BH/NS-WD binaries or be disrupted. In this section, we analyze the evolutionary routes leading to the formation of DCOs from wind-fed ULXs, with a particular attention placed on merging ones (mDCOs; i.e., with time to merger, $t_{\text{merge}} < 10$ Gyr).

Up to 46% of wind-fed ULXs (depending on the model) will form DCOs. Much fewer (up to 6%) represent progenitors of mDCOs (Table 2). Although the fractions of mDCO progenitors for tested models are different, all predict a similar expected number of these systems (about 1.4 per Milky Way-like galaxy). This happens because all of them are nearly exclusively powered through the BHL accretion mode and none are powered through WRLOF, the prescription for which presents the only difference between models. We note that nearly all ($\gtrsim 99\%$) of mDCO progenitors are wind-fed systems. Wind-powered systems can have much heavier donors ($M_{\text{ZAMS}} \gtrsim 8 M_{\odot}$; thus progenitors of compact objects) because the high mass-ratio ($\gtrsim 3$) does not lead to CE, which is an expected outcome if the RL is filled.

The small fraction of mDCO progenitors among ULXs results mainly from the preference for NS-forming donors in these systems¹¹ and the resulting disruption of the system (due to the natal kick). Even if such a system survives a supernova explosion without being disrupted, or it has evolved without a RLOF/CE phase, it will be (on average) too wide for a merger to occur within 10 Gyr; that is, $t_{\text{merger}} > 10$ Gyr.

The properties of mDCO progenitors are presented in Figure 8. The x -axis ranges remain the same as in the similar plots for the general distributions (Figure 7), so several distinct features are visible. Specifically, accretors are mostly BHs with a typical mass of 8–10 M_{\odot} , whereas donors are evolved Helium-rich stars with a typical mass of 5–7 M_{\odot} and very high luminosities ($\log_{10} L/L_{\odot} \approx 5$). These ULXs are typically very young objects with $t_{\text{age}} \ll 100$ Myr, so expected only in star-forming environments. Massive primaries and short orbital periods make the survival of the second SN more viable, but still most of these systems are disrupted (e.g., Wiktorowicz et al. 2019b).

Progenitors of mDCOs among wind-fed ULXs are mainly composed of a BH accretor with 8–9 M_{\odot} and a 5–7 M_{\odot}

evolved star that transfers mass through BHL mode. As stated earlier, there are no mDCO progenitors among ULXs powered through WRLOF mode because these are expanded post-MS stars on wide orbits and evolve typically into wide binaries with $t_{\text{merge}} \gg 10$ Gyr. In a typical case of a mDCO progenitor (Figure 9), both stars are initially relatively massive (49.0 M_{\odot} and 21.6 M_{\odot}), the separation is moderate ($a \approx 380 R_{\odot}$), and the orbit is nearly circular ($e \approx 0.03$). In about 4.4 Myr, the primary evolves off the MS and commences a MT onto the secondary, which leads to a mass reversal. In the next half Myr, the primary forms a BH with a mass of 8.14 M_{\odot} , while the orbit expands to 1800 R_{\odot} . The secondary needs an additional ~ 3 Myr to become a giant and fill its RL starting the CE phase, which results in a significant shrinkage of the separation (down to about 4.1 R_{\odot}). With its hydrogen layers ripped off, the secondary becomes a Helium MS star with a stellar wind that is strong enough to power a ULX though a BHL mode (MT rate of $1.8 \times 10^{-6} M_{\odot} \text{ yr}^{-1}$ out of which $\sim 15\%$ is transferred to the vicinity of the BH, which is enough to power an isotropic ULX). After about 0.7 Myr, it fills its RL and the MT mode switches to RLOF, which is much stronger and powers a hyper ULX (MT rate of $1.3 \times 10^{-3} M_{\odot} \text{ yr}^{-1}$ and luminosity of $L_{\text{X}} \approx 10^{42} \text{ erg s}^{-1}$). In a very short time (800 yr), the secondary explodes as a SN and forms a NS. The natal kick alters the orbit to a separation of 9.1 R_{\odot} and eccentricity of $e \approx 0.24$. The time to merger is $t_{\text{merge}} = 25.2$ Myr.

4. Discussion

4.1. Observed Systems

Although hundreds of ULXs have been detected so far (e.g., Walton et al. 2011; Swartz et al. 2011), only a handful of them have viable donor candidates. The observed donors can help us to understand the nature of ULXs, but are difficult-to-observe objects. Except for potential ULXs, such as SS433 and GRS1915, all (non Be-X) are extragalactic objects. Therefore, only the most luminous donors are bright enough to be identified by contemporary telescopes. The situations may be even worse given that binary evolution studies predict that most of the companions in ULXs, especially those containing NS accretors, have low masses and are still on their MS ($\lesssim 3 M_{\odot}$; Wiktorowicz et al. 2017). Additionally, in most situations, the spatial coincidence of a star and an X-ray source is the only argument for physical connection. Many ULXs (especially with visible—i.e., massive—donor candidates) are localized in dense, star-forming regions, where more than one star can exist in the X-ray position error circle. Furthermore, the accretion disk light may exceed the optical luminosity of the donor or be hard to remove from the photometry (e.g., Grisé et al. 2012; Sutton et al. 2014). Therefore, it is usually only possible to look for optical counterparts during the quiescent phases when the X-ray and optical emission from the disk is lowered.

Many authors have reported the detection of stars spatially coinciding with the X-ray sources, naming them companion candidates. Motch et al. (2011) identified a potential optical counterpart to NGC7793 P13 with spectral features suggesting a supergiant luminosity class. Motch et al. (2014) estimated a mass of 18–23 M_{\odot} for this object, assuming that minimum light represents the stellar light. Their modeling of the disk optical emission caused by X-ray heating supported this assumption. The star was classified as B9Ia, which together with the orbital period of ~ 64 days suggested the presence of a

¹¹ Companion stars in ULXs are typically secondaries (e.g., Wiktorowicz et al. 2017); that is, less-massive stars on ZAMS. For a uniform mass ratio distribution, the secondaries mass is typically half the mass of the primary. Therefore, if the secondary is to have an initial mass larger than $\sim 20 M_{\odot}$ (i.e., the lower limit for BH formation in isolation), then the primary should typically have an initial mass that is larger than about 40 M_{\odot} . Due to the steepness of the IMF, such primary masses are rare.

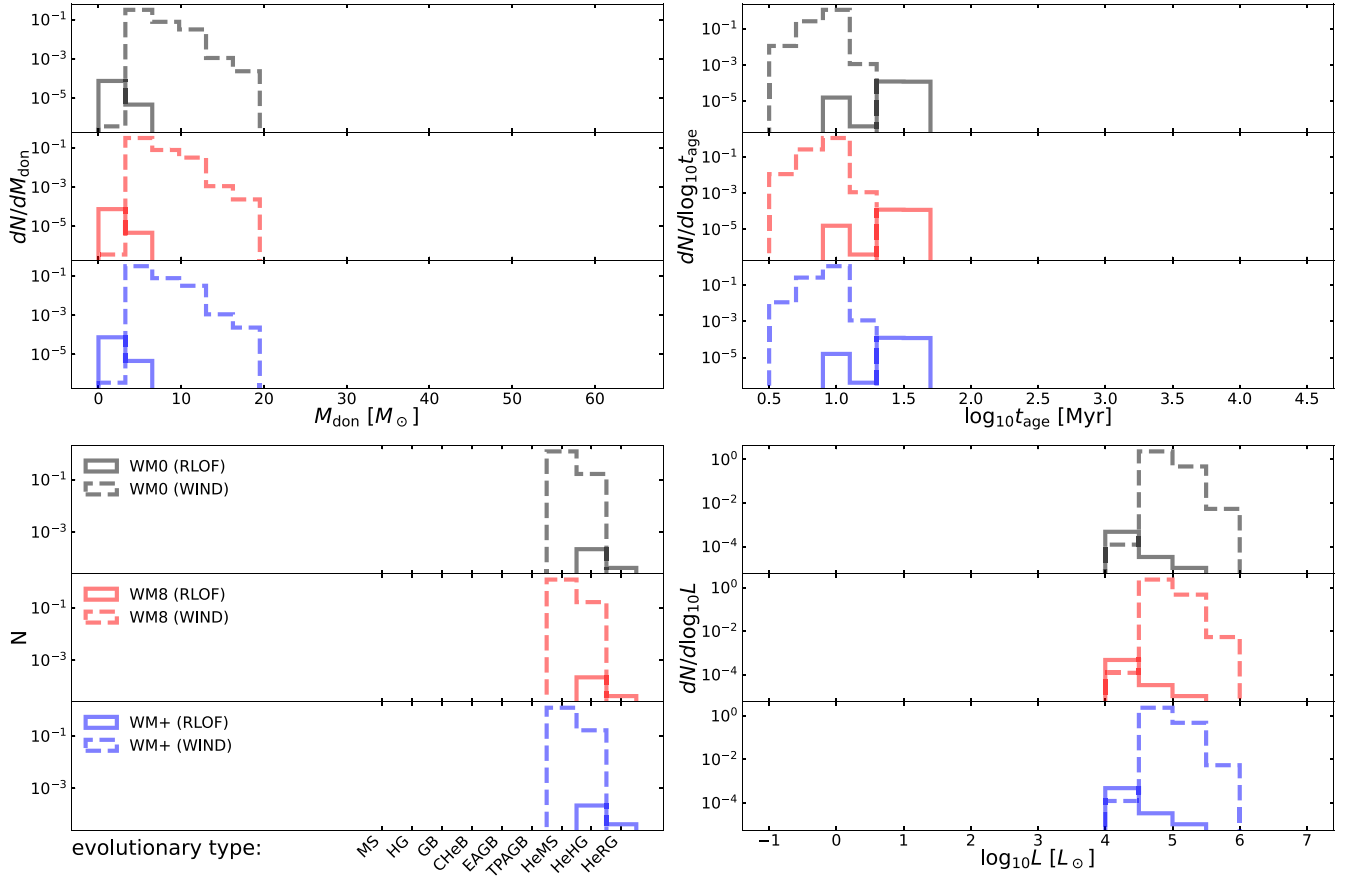


Figure 8. Parameter distributions of merging DCO progenitors among ULXs. Similar to Figure 7 (x -axes kept the same for easier comparison). There are no progenitors that are fed through WRLOF accretion mode, therefore, distributions for all tested models are similar.

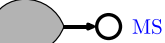
Merging DCO Progenitor Evolution					
age [Myr]		phase	$M_a [M_\odot]$	$M_b [M_\odot]$	
0	MS  MS $a \approx 380 R_\odot; e \approx 0.03$	ZAMS	49.0	21.6	
4.4	HG  MS $a \approx 420 R_\odot; e \approx 0.00$	MT	39.6 (14.3)	21.4 (25.4)	
5.0	BH  MS $a \approx 1,800 R_\odot; e \approx 0.00$	SN	8.14	25.2	
8.1	BH  CHeB $a \approx 4.1 R_\odot; e \approx 0.00$	CE	8.12	24.2	
8.4	BH  HeMS $a \approx 4.2 R_\odot; e \approx 0.00$	BHL	8.37 (8.56)	6.71 (5.36)	
9.1	BH  HeHG $a \approx 4.6 R_\odot; e \approx 0.00$	RLOF	8.56	5.36 (3.92)	
9.1	BH  NS $a \approx 9.1 R_\odot; e \approx 0.24$ $t_{\text{merge}} \approx 25.2 \text{ Myr}$	SN	8.56	1.45	

Figure 9. Same as Figure 4, but for a typical wind-fed ULX that is a progenitor of a merging DCO. Additional abbreviations (which are not explained in the captions to Figures 4, 5, and 6), are for binary evolution: CE—common envelope binary; and for stellar evolution: HeMS—Helium main sequence; HeHG—Helium Hertzsprung gap.

compact object with a mass less than $15 M_\odot$. Indeed, Fürst et al. (2016) discovered that it is a magnetized NS. Heida et al. (2014) concentrated on NIR companions to nearby (< 10 Mpc) ULXs and detected 11 potential NIR companions for 62 ULXs. They claim to detect all luminous NIR sources (RSG candidates) in this volume, which leads us to conclude that only a small fraction of ULXs are possibly accompanied by RSGs. Using this sample, Heida et al. (2015) identified a potential counterpart to the ULX in NGC 253 as a RSG candidate. The authors suggest that the unusually high proper motion ($\sim 66 \text{ km s}^{-1}$ larger than average for the Galaxy) strengthens their claim that the star and the ULXs are associated because such runaway RSGs are hard to explain otherwise. Heida et al. (2016) investigated five more ULXs from the Heida et al. (2014) sample and found that two of them are spatially coinciding with NIR sources that are compatible with being RSGs.

The study by Heida et al. (2014) was later extended by López et al. (2017) and King & Lasota (2020) to a final sample of 113 ULXs within the distance of 10 Mpc (from the total population of 170 ULXs in this range). In summary, viable RSG candidate counterparts were found for five of these ULXs.

Heida et al. (2019) identified a RSG spatially coinciding with NGC 300 ULX-1, which harbours a NS accretor (Carpano et al. 2018). For such a high mass-ratio, the orbital modulations of the donor candidate are expected to be immeasurable, despite the source being the nearest ULX with a known accretor type ($D = 2.0$ Mpc; Dalcanton et al. 2009).

Liu et al. (2013) detected a WR star in the ULXs in NGC 101, which provides MT onto the accretor through wind. The detection was based on spectroscopic analysis, so provides a stronger argument than just spatial coincidence.

For older environments the number of wind-fed ULXs is expected to drop significantly due to the short life span of supergiant stars, which constrain the majority of donors. Consequently, ULXs in old stellar populations (both RLOF- and wind-fed) are predicted to be dominated by NS accretors with low-mass donors ($\lesssim 3 M_{\odot}$; Wiktorowicz et al. 2017)

El Mellah et al. (2019) studied the importance of WRLOF on ULXs. They concentrated on two specific cases with mass ratios $q = 15$ and 2 . They analyzed NGC 7793 P13 and M101 ULX-1, and showed that their calculations agree with the systems being wind-fed ULXs for the known orbital parameters.

4.2. Wind Accretion Efficiency

In our results, the typical accretion efficiency in wind-fed ULXs in the BHL mode is 1%–2%, so only supergiants producing strong stellar wind can provide a MT rate large enough to power such a source. Meanwhile, in the WRLOF mode the accretion efficiency is much larger and typically reaches 30%–50%. However, for WRLOF to operate, the wind must be slow inside the RL, so again supergiants are the most promising donors. We note that 50% is a limit imposed on accretion efficiency in our reference model to avoid extrapolating the results of Mohamed (2010, see also Abate et al. 2013).

There are processes, which are not investigated in this study, that can decrease the efficiency of wind accretion. BHL is a simple model assuming the homogeneity of the accreted mass and a linear respective motion of the accretor and the gas. However, accretion in a binary system involves non-homogeneous winds, non-linear respective motions of the accretor and the wind-source (donor), as well as the presence of centrifugal forces. Theuns et al. (1996) performed a smooth particle hydrodynamic simulation of wind accretion in a situation where the orbital velocity is comparable to the wind velocity, and therefore cannot be neglected. They obtained mass-accretion rates 10 times smaller than expected from the BHL prescription. In addition, Boffin & Zacs (1994) noted that an order of magnitude lower mass-accretion rates give better agreement with observation of enrichment in barium stars. However, in the majority of our results, the orbits of wind-fed ULXs are wide, and therefore the wind velocity is much higher than the orbital velocity and the above effects may not be so strong.

For high mass-accretion rates ($\dot{M} \gtrsim \dot{M}_{\text{Edd}}$) the wake can become optically thick, which leads to instabilities that effectively reduce the accretion rate because of radiation momentum and energy deposition in the flow (Taam et al. 1991). Furthermore, Bermúdez-Bustamante et al. (2020) showed that in AGB stars, most of the wind is lost through the L2 point and forms an excretion disk around the binary, effectively reducing the MT rate.

A detailed treatment of the accretion process may also lead to an increase of the wind accretion rates. For example, the formation of an accretion disk is an effect that has been ignored in the analytical solutions but which proved to be potentially important in hydrodynamical simulations, and can occur also in the BHL accretion mode (Theuns et al. 1996). The disk can

help to reduce the angular momentum of the accretion flow and, consequently, increase the accretion rate. Furthermore, the accretion flow can be heated to a high temperature while the gravitational energy is being released, which can result in the production of highly-energetic radiation that can irradiate the donor, and thus increase its mass-loss rate. Unfortunately, hydrodynamical simulations cover only a small fraction of the parameter space and these results cannot be applied to a general case.

Similarly, the available hydrodynamical simulations of WRLOF accretion flows are scarce and the analytical fits, such as those of Abate et al. (2013), depend on restricting assumptions. In particular, the upper limit for the fraction of accreted mass can be higher than 50% and a WRLOF may smoothly convert into a RLOF when the star fills its RL.

4.3. Spatial Coincidence Probability for ULXs and RSGs

Heida et al. (2015) investigated a ULX in NGC 273 (designated as J0047) that has a spatially coinciding RSG donor candidate. They calculated the probability that J0047 and the RSG are only located in the same place on the sky by chance as $< 2.6\%$ through dividing the X-ray detection error circle (95% credibility) by the size of the observational field and multiplying this value by the number of RSGs (not-fainter than the RSG coinciding with J0047) in this field. This approach was later used for two other ULXs with spatially coinciding RSGs in Heida et al. (2016).

We note that such an approach does not give a probability for spatial coincidence, which is a general concept for a population, but only gives an expected number of RSGs with this specific luminosity inside randomly located X-ray detection error circle for this particular field. It can be shown that by performing the same analysis for a (possibly imaginary) field with $\gtrsim 100$ times more RSGs, the procedure predicts a superposition chance above 100%.

The main problem of this method is that the object chosen for investigation (J0047) was not chosen at random, but due to the coinciding RSG. This is a relatively rare situation because only several such cases were found among hundreds of known ULXs. Only the analysis of the entire populations of ULXs and RSGs, or their representative samples, may allow us to perform reliable statistical estimates of the probability of having a ULX and a RSG in the same position on the sky. The situation may be further complicated by the fact that current observational surveys are biased toward bright NIR sources, effectively favoring RSGs while neglecting other unobserved stars that may be much better donor candidates.

Recently, King & Lasota (2020) performed a combined analysis for 113 nearby ULXs, focusing on deriving the expected number of RSGs spatially coinciding with this sample. They obtained the expected number of 3.7 such coincidences, which is of the same order as the number of ULX with RSG donor candidates (five systems) in their sample.

Despite the problems pointed out above with connecting ULXs to RSGs by spatial coincidence alone, we note that our theoretical analysis presented in this paper shows that a significant fraction of the ULXs ($\sim 42\%$ – 54% ; Table 2) possess RSG donors. Some of these sources may be hidden from our view because of misalignment of the emission beam and the line of sight.

5. Summary

In this study, we analyzed the population of wind-fed ULXs in the context of the entire ULX population. Using the population synthesis method and statistical analysis, we showed that wind-fed ULXs, which were mostly neglected in previous studies, constitute a significant fraction of all ULXs and in some environments may be a majority. Although our assumptions were rather optimistic, we prove that wind-fed ULXs cannot be neglected in research on ULXs, lest the study be systematically biased. Our sample contains a significant fraction of RSG companions, and thus supports the suggestion that the apparent superposition of some ULXs and RSGs results from coexistence as a binary. Although some of these systems will evolve into DCOs, none of the ULX systems harboring a RSG donor are viable progenitors of DCO mergers with $t_{\text{merge}} < 10$ Gyr, due to the large separations.

It should be stressed that the models of wind accretion and emission that are used in our study might not always be realistic, which could influence our results. This problem cannot be solved by extensive numerical simulations alone, and requires us to obtain quantitative and qualitative observational data.

We are thankful to the anonymous referee who pointed out relevant points to make the paper more consistent. We also thank the thousands of volunteers who took part in the *Universe@Home* project¹² and who provided their computers for the simulation used in this study. G.W. is partly supported by the President's International Fellowship Initiative (PIFI) of the Chinese Academy of Sciences under grant no. 2018PM0017 and by the Strategic Priority Research Program of the Chinese Academy of Science Multi-wave band Gravitational Wave Universe (grant No. XDB23040000). This work is partly supported by the National Natural Science Foundation of China (grant No. 11690024, 11873056, and 11991052) and the National Key Program for Science and Technology Research and Development (grant No. 2016YFA0400704). K.B. and G.W. acknowledge the NCN grant MAESTRO 2018/30/A/ST9/00050. This work is partly supported by the National Key Program for Science and Technology Research and Development (grant No. 2016YFA0400704), and the National Natural Science Foundation of China (grant No. 11690024 and 11873056). J.P.L. was supported in part by a grant from the French Space Agency CNES. K.B. acknowledges support from the Polish National Science Center (NCN) grant Maestro (2018/30/A/ST9/00050).

ORCID iDs

Grzegorz Wiktorowicz  <https://orcid.org/0000-0001-6106-0515>

Jean-Pierre Lasota  <https://orcid.org/0000-0002-6171-8396>

Youjun Lu  <https://orcid.org/0000-0002-1310-4664>

Krystian Iłkiewicz  <https://orcid.org/0000-0002-4005-5095>

References

Abate, C., Pols, O. R., Izzard, R. G., Mohamed, S. S., & de Mink, S. E. 2013, *A&A*, **552**, A26
 Abbott, B. P., Abbott, R., Abbott, T. D., et al. 2016, *ApJL*, **818**, L22

Abbott, R., Abbott, T. D., LIGO Scientific Collaboration, et al. 2020, *ApJL*, **896**, L44
 Abramowicz, M. A. 2005, in *Growing Black Holes: Accretion in a Cosmological Context*, ed. A. Merloni, S. Nayakshin, & R.A. Sunyaev (Berlin: Springer), 257
 Bachetti, M., Harrison, F. A., Walton, D. J., et al. 2014, *Natur*, **514**, 202
 Belczynski, K. 2020, *ApJL*, **905**, L15
 Belczynski, K., Bulik, T., Fryer, C. L., et al. 2010a, *ApJ*, **714**, 1217
 Belczynski, K., Dominik, M., Bulik, T., et al. 2010b, *ApJL*, **715**, L138
 Belczynski, K., Kalogera, V., Rasio, F. A., et al. 2008, *ApJS*, **174**, 223
 Belczynski, K., Klencki, J., Fields, C. E., et al. 2020, *A&A*, **636**, A104
 Bermúdez-Bustamante, L. C., García-Segura, G., Steffen, W., & Sabin, L. 2020, *MNRAS*, **493**, 2606
 Boffin, H. M. J., & Jorissen, A. 1988, *A&A*, **205**, 155
 Boffin, H. M. J., & Zacs, L. 1994, *A&A*, **291**, 811
 Bondi, H. 1952, *MNRAS*, **112**, 195
 Brightman, M., Earnshaw, H., Fürst, F., et al. 2020, *ApJ*, **895**, 127
 Brightman, M., Harrison, F. A., Fürst, F., et al. 2018, *NatAs*, **2**, 312
 Carpano, S., Haberl, F., Maitra, C., & Vasilopoulos, G. 2018, *MNRAS*, **476**, L45
 Chandra, A. D., Roy, J., Agrawal, P. C., & Choudhury, M. 2020, *MNRAS*, **495**, 2664
 Colbert, E. J. M., & Mushotzky, R. F. 1999, *ApJ*, **519**, 89
 Copperwheat, C., Cropper, M., Soria, R., & Wu, K. 2005, *MNRAS*, **362**, 79
 Copperwheat, C., Cropper, M., Soria, R., & Wu, K. 2007, *MNRAS*, **376**, 1407
 Dalcanton, J. J., Williams, B. F., Seth, A. C., et al. 2009, *ApJS*, **183**, 67
 Dall'Osso, S., Perna, R., & Stella, L. 2015, *MNRAS*, **449**, 2144
 Earnshaw, H. P., Heida, M., Brightman, M., et al. 2020, *ApJ*, **891**, 153
 Edgar, R. 2004, *NewAR*, **48**, 843
 Ekşi, K. Y., Andaç, İ. C., Çıkıntoğlu, S., et al. 2015, *MNRAS*, **448**, L40
 El Mellah, I., Sundqvist, J. O., & Keppens, R. 2019, *A&A*, **622**, L3
 Fürst, F., Walton, D. J., Harrison, F. A., et al. 2016, *ApJL*, **831**, L14
 Fürst, F., Walton, D. J., Stern, D., et al. 2017, *ApJ*, **834**, 77
 Greene, J. E., Strader, J., & Ho, L. C. 2020, *ARA&A*, **58**, 257
 Grisé, F., Kaaret, P., Corbel, S., et al. 2012, *ApJ*, **745**, 123
 Hamann, W. R., & Koesterke, L. 1998, *A&A*, **335**, 1003
 Hameury, J. M., & Lasota, J. P. 2020, *A&A*, **643**, A171
 Heida, M., Jonker, P. G., Torres, M. A. P., et al. 2014, *MNRAS*, **442**, 1054
 Heida, M., Jonker, P. G., Torres, M. A. P., et al. 2016, *MNRAS*, **459**, 771
 Heida, M., Lau, R. M., Davies, B., et al. 2019, *ApJL*, **883**, L34
 Heida, M., Torres, M. A. P., Jonker, P. G., et al. 2015, *MNRAS*, **453**, 3510
 Höfner, S. 2007, in *ASP Conf. Ser.*, 378, *Headwind: Modelling Mass Loss of AGB Stars, Against All Odds*, ed. F. Kerschbaum, C. Charbonnel, & R. F. Wing (San Francisco, CA: ASP), 145
 Höfner, S., & Olofsson, H. 2018, *A&ARv*, **26**, 1
 Hoyle, F., & Lyttleton, R. A. 1939, *PCPS*, **35**, 405
 Hurley, J. R., Pols, O. R., & Tout, C. A. 2000, *MNRAS*, **315**, 543
 Iłkiewicz, K., Mikołajewska, J., Belczyński, K., Wiktorowicz, G., & Karczmarek, P. 2019, *MNRAS*, **485**, 5468
 Israel, G. L., Belfiore, A., Stella, L., et al. 2017, *Sci*, **355**, 817
 Ivanova, N., Justham, S., Chen, X., et al. 2013, *A&ARv*, **21**, 59
 Kaaret, P., Feng, H., & Roberts, T. P. 2017, *ARA&A*, **55**, 303
 King, A., & Lasota, J.-P. 2005, *A&A*, **442**, 587
 King, A., & Lasota, J.-P. 2019, *MNRAS*, **485**, 3588
 King, A., & Lasota, J.-P. 2020, *MNRAS*, **494**, 3611
 King, A., & Lasota, J.-P. 2020, *MNRAS*, **497**, 917
 King, A. R. 2009, *MNRAS*, **393**, L41
 King, A. R., Davies, M. B., Ward, M. J., Fabbiano, G., & Elvis, M. 2001, *ApJL*, **552**, L109
 Kippenhahn, R., Kohl, K., & Weigert, A. 1967, *ZAp*, **66**, 58
 Kippenhahn, R., & Weigert, A. 1967, *ZAp*, **65**, 251
 Lasota, J.-P., Vieira, R. S. S., Sadowski, A., Narayan, R., & Abramowicz, M. A. 2016, *A&A*, **587**, A13
 Liao, Z., Liu, J., Zheng, X., & Gou, L. 2020, *MNRAS*, **492**, 5922
 Licquia, T. C., & Newman, J. A. 2015, *ApJ*, **806**, 96
 Liu, J.-F., Bregman, J. N., Bai, Y., Justham, S., & Crowther, P. 2013, *Natur*, **503**, 500
 López, K. M., Heida, M., Jonker, P. G., et al. 2017, *MNRAS*, **469**, 671
 Maxted, N. I., Ruiters, A. J., Belczynski, K., Seitzzahl, I. R., & Crocker, R. M. 2020, *arXiv:2010.15341*
 Middleton, M. J., Brightman, M., Pintore, F., et al. 2019, *MNRAS*, **486**, 2
 Middleton, M. J., Heil, L., Pintore, F., Walton, D. J., & Roberts, T. P. 2015, *MNRAS*, **447**, 3243
 Mohamed, S. 2010, PhD thesis, University of Oxford

¹² <https://universeathome.pl/>

- Mohamed, S., & Podsiadlowski, P. 2007, in ASP Conf. Ser., 372, 15th European Workshop on White Dwarfs, ed. R. Napiwotzki & M. R. Burleigh (San Francisco, CA: ASP), 397
- Mondal, S., Belczynski, K., Wiktorowicz, G., Lasota, J.-P., & King, A. R. 2020, *MNRAS*, 491, 2747
- Motch, C., Pakull, M. W., Grisé, F., & Soria, R. 2011, *AN*, 332, 367
- Motch, C., Pakull, M. W., Soria, R., Grisé, F., & Pietrzyński, G. 2014, *Natur*, 514, 198
- Mushtukov, A. A., Suleimanov, V. F., Tsygankov, S. S., & Poutanen, J. 2015, *MNRAS*, 454, 2539
- Paczynski, B. 1971, *ARA&A*, 9, 183
- Pakull, M. W., Grisé, F., & Motch, C. 2006, in IAU Symp. 230, Populations of High Energy Sources in Galaxies, ed. E. J. A. Meurs & G. Fabbiano (Cambridge: Cambridge Univ. Press), 293
- Pavlovskii, K., Ivanova, N., Belczynski, K., & Van, K. X. 2017, *MNRAS*, 465, 2092
- Poutanen, J., Lipunova, G., Fabrika, S., Butkevich, A. G., & Abolmasov, P. 2007, *MNRAS*, 377, 1187
- Rodríguez Castillo, G. A., Israel, G. L., Belfiore, A., et al. 2020, *ApJ*, 895, 60
- Sathyaprakash, R., Roberts, T. P., Walton, D. J., et al. 2019, *MNRAS*, 488, L35
- Shakura, N. I., & Sunyaev, R. A. 1973, *A&A*, 24, 337
- Shima, E., Matsuda, T., Takeda, H., & Sawada, K. 1985, *MNRAS*, 217, 367
- Sutton, A. D., Done, C., & Roberts, T. P. 2014, *MNRAS*, 444, 2415
- Swartz, D. A., Soria, R., Tennant, A. F., & Yukita, M. 2011, *ApJ*, 741, 49
- Taam, R. E., Fu, A., & Fryxell, B. A. 1991, *ApJ*, 371, 696
- Tetarenko, B. E., Sivakoff, G. R., Heinke, C. O., & Gladstone, J. C. 2016, *ApJS*, 222, 15
- Theuns, T., Boffin, H. M. J., & Jorissen, A. 1996, *MNRAS*, 280, 1264
- Tong, H. 2015, *RAA*, 15, 517
- Tsygankov, S. S., Doroshenko, V., Lutovinov, A. A., Mushtukov, A. A., & Poutanen, J. 2017, *A&A*, 605, A39
- van den Heuvel, E. P. J., Portegies Zwart, S. F., & de Mink, S. E. 2017, *MNRAS*, 471, 4256
- Vink, J. S. 2008, *NewAR*, 52, 419
- Vink, J. S., & de Koter, A. 2002, *A&A*, 393, 543
- Vink, J. S., de Koter, A., & Lamers, H. J. G. L. M. 2001, *A&A*, 369, 574
- Walton, D. J., Bachetti, M., Fürst, F., et al. 2018, *ApJL*, 857, L3
- Walton, D. J., Roberts, T. P., Mateos, S., & Heard, V. 2011, *MNRAS*, 416, 1844
- Wiktorowicz, G., Wyrzykowski, Ł., Chruslinska, M., et al. 2019b, *ApJ*, 885, 1
- Wiktorowicz, G., Lasota, J.-P., Middleton, M., & Belczynski, K. 2019a, *ApJ*, 875, 53
- Wiktorowicz, G., Sobolewska, M., Lasota, J.-P., & Belczynski, K. 2017, *ApJ*, 846, 17
- Wiktorowicz, G., Sobolewska, M., Sądowski, A., & Belczynski, K. 2015, *ApJ*, 810, 20
- Zdziarski, A. A. 2014, *MNRAS*, 444, 1113